# Surface-structure analysis of Au overlayers on Si by impact-collision ion-scattering spectroscopy: $\sqrt{3}\times\sqrt{3}$ and $6\times6$ Si(111)/Au

Judy H. Huang and R. Stanley Williams
*Department of Chemistry and Biochemistry and Solid State Science Center, University of California, Los Angeles, California 90024*
(Received 26 January 1988)

Amounts of Au equivalent to about 0.8 monolayer and 1.1 monolayers have been deposited onto Si(111) surfaces, and after annealing to 700 °C the atomic structures of the adatom-induced reconstructions ($\sqrt{3}\times\sqrt{3}$ and $6\times6$, respectively) have been studied using primarily impact-collision ion-scattering spectroscopy (ICISS). The ion-scattering results were quantitatively analyzed by comparing them to the results of computer simulations for various structural models. The scattered-ion angular distributions clearly show that the Au atoms are not embedded in the Si surface, and the underlying Si atoms are not displaced markedly from their bulk positions. Two types of Au adatoms are found on both surfaces: those that are located $2.0\pm0.2$ Å above the outermost Si plane at threefold hollow sites and are arranged in a honeycomb network, and those that reside in the centers of the honeycomb hexagons $0.3\pm0.05$ Å below the honeycomb plane. A model is proposed that is consistent with both the ICISS and low-energy electron-diffraction results: The $\sqrt{3}\times\sqrt{3}$ surface is essentially an incomplete $6\times6$ structure with little ordering of the empty honeycomb and centered-hexagon units, whereas the $6\times6$ surface is predominantly covered by centered hexagons with the empty honeycomb units ordered in a regular array.

## I. INTRODUCTION

The detailed atomic structure of metal-Si interfaces has become a subject of major interest. A great deal of effort has been focused on the Au/Si(111) system,[1,2] but there is still no consensus about the atomic structure of the various reconstructions that are observed. One crucial point is the extent of intermixing between the metal and Si; the formation of "gold silicide" or an interfacial compound with a maximum thickness of 30 Å has been postulated.[1,3] However, the binary Au-Si phase diagram does not display any intermetallic compounds, and the mutual solid solubilities are very small (about $10^{-16}$ cm$^{-3}$ of Au in Si at 1150 °C).[4]

To clarify these issues, determination of the atomic geometry for submonolayer Au coverages on the Si(111) surface is of great importance. Au-on-Si(111) surfaces have been reported to be reconstructed into $5\times1$, $\sqrt{3}\times\sqrt{3}$, and $6\times6$ structures, depending on the amount of Au deposited and the annealing conditions.[1-8] A similar sample preparation procedure also produces a $\sqrt{3}\times\sqrt{3}$ structure for the Ag/Si(111) system,[1] which has also merited special attention. A review of both systems and details of many of the reconstructions postulated for these surfaces can be found in Ref. 1.

Many different structural models for the $\sqrt{3}\times\sqrt{3}$ and $6\times6$ Si(111) surfaces have been proposed in both theoretical and experimental studies. They can be divided roughly into two categories: models with adatoms that sit above the Si(111) surface and those with Ag or Au embedded into or below the topmost Si layer. These models can be further classified as follows: simple honeycomb,[1,9-11] centered hexagon,[1,12] various trimers,[1,6,7,11-15] threefold substitutional,[11] surface-embedded Au,[16,17] and subsurface-immersed Au.[18] A well-ordered $6\times6$ structure for the higher coverages of Au on Si(111) has been proposed by Higashiyama, Kono, and Sagawa,[19] based on a structure with local $\sqrt{3}\times\sqrt{3}$ symmetry obtained by Salvan *et al.*[20] Le Lay has concluded that the $6\times6$ structure is a Au-Si two-dimensional compound with a composition close to that of the bulk Si-Au eutectic compound.[7,15]

For $\sqrt{3}\times\sqrt{3}$ models with the metal atoms located above the Si(111) surface, there have been debates on which adsorption site, i.e., the simple atop (directly above a surface Si), threefold atop (above a second layer Si), threefold hollow, or various trimers, is the most stable.[11] In the first report of the $\sqrt{3}\times\sqrt{3}$ Ag surface in a uv-photoemission spectroscopy (UPS) and Auger-electron spectroscopy (AES) study, a trimer model in which the Ag atoms are centered over a second-layer Si atom was proposed.[21] This model was supported in subsequent studies using reflection high-energy-electron diffraction (RHEED)[6] and electron-energy-loss spectroscopy (ELS) with UPS and AES,[7,15] with perhaps some minor modifications. A different trimer model[14] with the atoms clustered over threefold-hollow sites was suggested in a study by impact-collision ion-scattering spectroscopy (ICISS).

A surface-enhanced x-ray-absorption fine-structure (SEXAFS) study by Stohr *et al.*[11] supported a threefold-hollow site for Ag on Si(111). A honeycomb arrangement of adatoms was favored in experimental studies utilizing ICISS (Ref. 9) and scanning tunneling microscopy (STM).[10] In a quantum-mechanical cluster calculation for Si(111)/Ag,[12] a self-consistent Hartree-Fock method was used and the results favored a threefold site over the simple atop site for the local adsorption site. This report

 

also supported a honeycomb arrangement of the Ag atoms, and introduced a centered-hexagon model, in which the central atom is displaced somewhat lower than the six atoms forming the hexagon, for surfaces with higher coverages. The SEXAFS study[11] of Si(111)/Ag eliminated the possibility of simple-atop, trimer, and threefold-atop local adsorption sites, but suggested the possibility that on annealed surfaces the adatoms could be below the top Si layer in a threefold-hollow region.

Often, the same techniques used by researchers who concluded that Au or Ag must sit above the Si(111) surface were used by others who concluded that Au must sit below the surface. A subsurface-immersed Au model was reported in a low-energy ion-scattering (LEIS) study,[18] and a surface-embedded trimer model was favored in a STM study[16] of Si(111)/Ag in which the data were essentially identical to those in Ref. 10. Despite all the effort put into the determination of the Ag and Au/Si(111) atomic structures, no one model is clearly favored at this time. The intent of this paper is thus to determine the actual atomic structure of the $\sqrt{3}\times\sqrt{3}$ and $6\times6$ Si(111)/Au surfaces, realizing that the Si(111)/Ag surface may have a different structure.

In the present study, the $\sqrt{3}\times\sqrt{3}$ and $6\times6$ reconstructions were prepared by evaporating specific amounts of Au onto clean $7\times7$ Si(111) surfaces. The resulting systems were studied with low-energy electron diffraction (LEED) and ICISS. In ICISS, which was developed by Aono *et al.*,[22–24] the experimental scattering angle is fixed close to 180° to ensure that the detected ions have scattered from near-surface atoms with nearly zero impact parameter. This specialization of the scattering condition minimizes the contribution of multiple scattering to the detected yield and simplifies the interpretation of the angular dependence of the backscattered yield as a function of the sample orientation with respect to the ion beam.

In the ICISS polar scans obtained for this study, 5-keV $Li^+$ ions were used as projectiles instead of $He^+$. The path-dependent neutralization rate is much larger for $He^+$ than $Li^+$,[25] so the large dose of $He^+$ necessary to obtain results with reasonable signal-to-noise level may damage the surface before a complete data set can be collected if the detector is an electrostatic analyzer. Using $He^+$ ions for ICISS results in a much higher surface sensitivity, but backscattered $Li^+$ ions produce much more distinct flux peaks. This makes the interpretation of $Li^+$-scattering data less uncertain than for $He^+$, since the Auger neutralization lifetime of $He^+$ is in general not known and local neutralization effects can introduce structure in the ICISS angular scans that may be mistaken for shadowing or blocking effects.[24]

Because of the mass dispersion and short-range structural sensitivity of ion scattering, ICISS has been shown to be ideally suited for the study of a metal overlayer on a semiconductor surface for the case of $NiSi_2$ on Si(001).[26] The $Li^+$ ion-scattering results for $NiSi_2$(001) clearly showed that Si atoms were in the outermost atomic plane and that Ni resided in the second layer and also provided quantitative information about the interlayer separation and the surface vacancy concentration.[26] The ICISS polar scans were analyzed by comparing them with computer simulations of scattering probabilities,[25,27–29] which have also been applied in the quantitative analysis of the Au-on-Si(111) surface in this study.

A unified structural model of the $\sqrt{3}\times\sqrt{3}$ and $6\times6$ Si(111)/Au surfaces incorporating a framework of the simple honeycomb structure with different filling of the hexagons yields excellent agreement with our results. The honeycomb Au atoms are located in threefold-hollow sites $2.0\pm0.2$ Å above the Si(111) surface, and the Au atoms at the hexagon centers are $0.3\pm0.05$ Å below the honeycomb plane. The $\sqrt{3}\times\sqrt{3}$ is essentially an incomplete and somewhat disordered $6\times6$. In the next section, the details of the experimental procedure are described. The experimental results along with their qualitative interpretation are presented in Sec. III. The ICISS calculations and their quantitative analysis are discussed in Sec. IV. Finally, the conclusions of this work are presented in Sec. V.

## II. EXPERIMENT

Si(111) samples ($5\times10\times0.5$ mm$^3$) were cleaned by annealing in the ultrahigh vacuum (UHV) ion-scattering chamber at about 450 °C for 15 min and flash heated to about 1000° C for 3 sec. No HF solution was used to remove the native oxide layer before the samples were loaded into the UHV chamber. This procedure produced a sharp $7\times7$ LEED pattern and no detectable contamination in Auger spectra was recorded after cooling the samples to room temperature (RT). The LEED pattern was also used to align the azimuthal orientation of the sample prior to collecting ICISS angular scans.

The Au films on Si(111) were prepared by solid-phase epitaxy (SPE), in which Au was evaporated onto the RT Si substrate by directly heating a Au wire wrapped around a tungsten filament. The pressure in the UHV chamber was below $4\times10^{-9}$ Torr during Au deposition. The rate of deposition, which was measured with an Inficon XTM thin-film monitor, was approximately 0.1 monolayers (ML) per minute. After the desired amount of Au had been deposited, the samples were annealed by resistively heating at about 700 °C for 10 min. During all heat treatments, the sample temperature was checked using both infrared and optical pyrometers.

Surfaces with approximately 0.80 and 1.10 ML of Au were prepared on different $7\times7$ Si(111) samples to produce the best $\sqrt{3}\times\sqrt{3}$ and $6\times6$ LEED structures, respectively. These Au coverages were experimentally found to produce the most distinct LEED patterns. It was not possible to obtain a clean and well-ordered $7\times7$ Si(111) surface by sputtering and annealing a Au-covered surface, so a fresh substrate had to be used for each experiment. LEED *I-V* spectra for the (1,0) beams from each surface were obtained from 50 to 150 eV in 2-eV increments by integrating 500 video frames at each energy using a video camero interfaced to a computer-controlled digitization system, as described in Ref. 26.

The ion scattering chamber is coupled to a 30-keV ion accelerator with a Colutron ion source.[25,26] The base pressure of the chamber was $2\times10^{-11}$ Torr after the

samples had been prepared and examined by LEED. During the ion-scattering measurements, the pressure rose to about $5\times10^{-10}$ Torr. Both lithium and helium ions at 5 keV kinetic energy were used as projectiles, and backscattered ions were analyzed with a hemispherical electrostatic analyzer (ESA), which could be rotated to intercept scattering angles from 0° to 166°. The ESA was operated in the constant pass energy mode (1500 eV) with an energy resolution of about 20 eV. Before each ICISS polar scan was collected, an energy spectrum of the backscattered ions at normal incidence was collected to determine the energy of the elastically scattered ions from Au and Si. The analyzer energy was set to the energy of the maximum intensity for the Au or Si peak. The ICISS polar scans were then collected by measuring the intensity of $Li^+$ ions, initially incident at 5 keV, scattered elastically from Au or Si atoms into the electrostatic analyzer at an angle of 157° as a function of the polar angle (the angle between the surface plane and the ion beam) from 0° to 90° in 2° increments. Data were collected with the ion beam initially incident along four different azimuthal orientations, namely $[1\,1\,\bar{2}]$, $[\bar{1}\,\bar{1}\,\bar{2}]$, $[1\,\bar{1}\,0]$, and $[\bar{1}\,1\,0]$.

## III. RESULTS AND QUALITATIVE ANALYSES

The LEED integral-order and fractional-order spots of the $\sqrt{3}\times\sqrt{3}$ and $6\times6$ structures were distinct and intense. The LEED *I-V* spectra for the (1,0) beam at normal electron incidence are presented in Fig. 1 for both structures. The raw experimental data are presented to enable other workers to compare their results to ours. As shown in Fig. 1, the *I-V* curves for the (1,0) spot were very similar for the two reconstructions, which indicates that the structures of the two surfaces should be similar. Figure 2 presents typical LEED spot profiles plotted as intensity versus relative momentum transfer. All the LEED spots were sharp, but the characteristic length scale of the ordered regions producing the fractional order spots was roughly 340 and 610 Å for the $\sqrt{3}\times\sqrt{3}$ and the $6\times6$ structures, respectively. The panel in Fig. 2(a) compares fractional order spots from the two surfaces on the same momentum scale and shows that the $\sqrt{3}\times\sqrt{3}$ spots, which were narrowest at this particular Au coverage, are considerably broader than the $6\times6$ spots. Thus the $6\times6$ surface has much longer-range ordering than that of the $\sqrt{3}\times\sqrt{3}$.

LEIS energy spectra for 5-keV $Li^+$ ions scattered at 165° and 97° from the $6\times6$ structure are presented in Fig. 3. The $\sqrt{3}\times\sqrt{3}$ structure yielded essentially identical spectra. Ions incident along the sample normal were scattered elastically by atoms at the surface region, giving rise to a surface peak (SP) for both Au and Si. As shown in Fig. 3(a), $Li^+$ ions backscattered from Si atoms at 165° produced both a SP due to single scattering and an extended background resulting from multiple scattering. The $Li^+$ ions that scattered from Au atoms produced only a sharp SP, indicating that the Au atoms for this

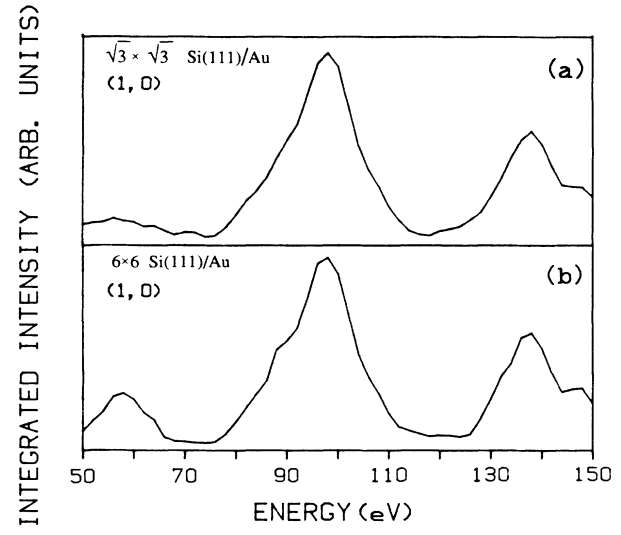


FIG. 1. Experimental LEED *I-V* spectra from $\sqrt{3}\times\sqrt{3}$ Si(111)/Au (a) and $6\times6$ Si(111)/Au (b) at normal electron-beam incidence for the (1,0) beam. The only difference in the two spectra is that the feature centered at 58 eV is more intense for the $6\times6$ surface.

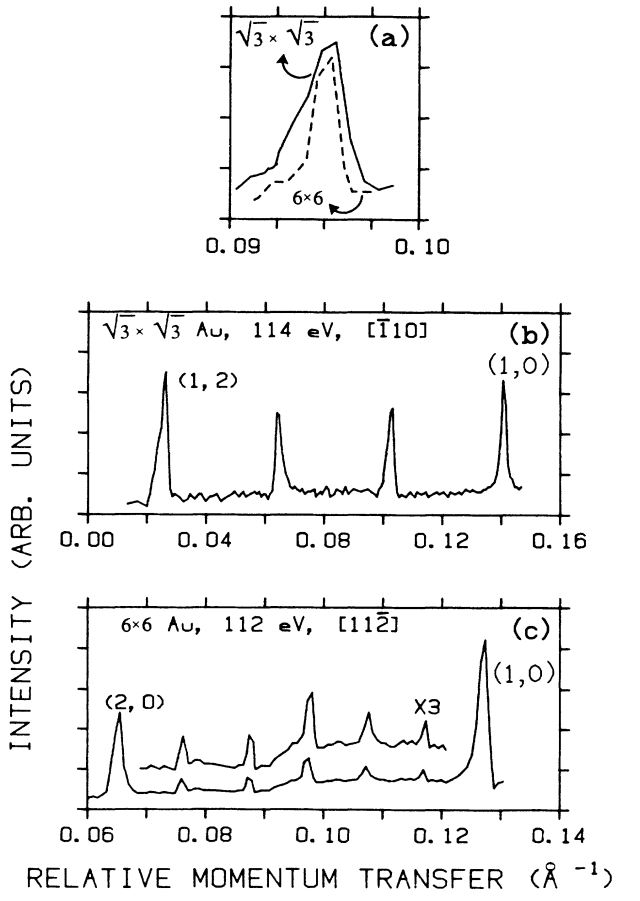


FIG. 2. LEED spot profiles at normal incidence for Si(111)/Au: (a) comparison of fractional-order spots for the $\sqrt{3}\times\sqrt{3}$ (solid line) and $6\times6$ (dashed line) surfaces, (b) for the $\sqrt{3}\times\sqrt{3}$ through the center of the (1,0) and (1,2) spots, and (c) for the $6\times6$ surface through the (1,0) and (2,0) spots. The ordinate is a relative momentum transfer, expressed in $Å^{-1}$. Note that the azimuthal orientations for the two profiles (b) and (c) are rotated 30° with respect to each other.

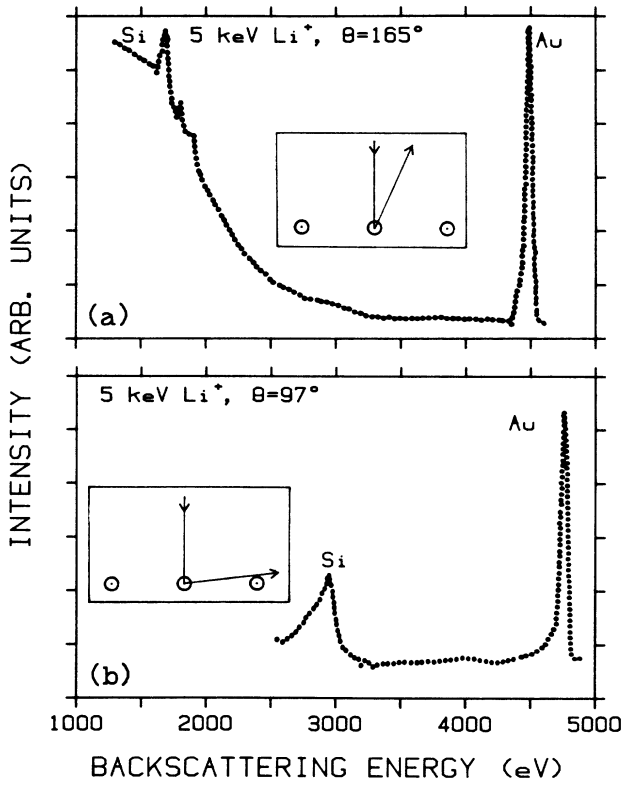


FIG. 3. Energy spectra of 5-keV lithium ions backscattered from the $6\times6$ Si(111)/Au surface for normal ion incidence. The scattering angle ($\theta$), which is measured between the analyzer and the projectile trajectory through the sample, is (a) 165° and (b) 97°. The insets show the ion incidence and scattering geometries. Both Au and Si surface peaks (SP) are present in each spectrum.

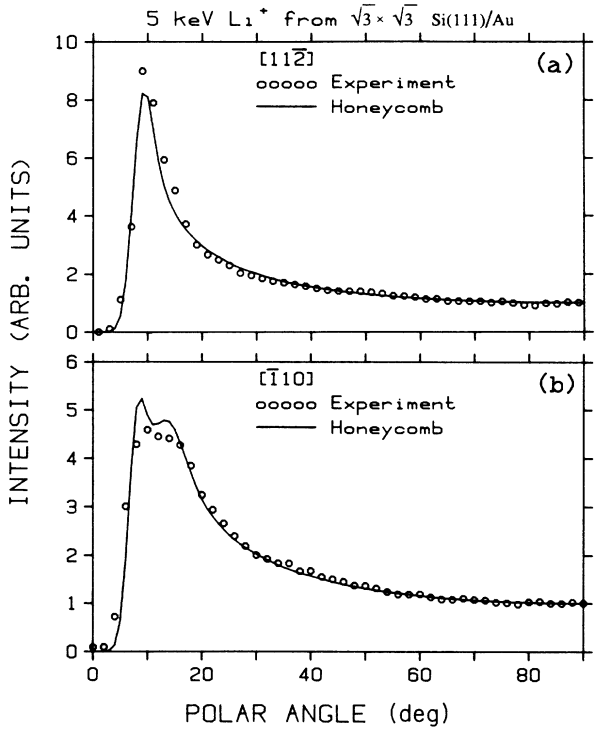


FIG. 4. Experimental ICISS polar scan (○) for 5-kEV $Li^+$ scattering at 157° from the Au atoms on the $\sqrt{3}\times\sqrt{3}$ Si(111)/Au surface along the (a) $[1\,1\,\bar{2}]$ and (b) $[\bar{1}\,1\,0]$ azimuths. The solid lines are the result of a calculation for a honeycomb structure. The ordinate refers to the calculated intensity. The calculated distribution was normalized to the experimental intensity at the polar angle of 90°.

coverage were in a well-defined layer and not interdiffused with Si.

Figure 3(b) shows the energy spectrum for 5-keV $Li^+$ scattered at 97° along the $[1\,1\,\bar{2}]$ azimuth. For this geometry, the scattered ions must exit the surface at a grazing angle, which strongly enhances the yield from the surface plane. The Au SP was still intense, which demonstrated that blocking of $Li^+$ ions backscattered from Au by neighboring Au or Si atoms was negligible. However, the elastic scattering from Si was severely attenuated, which indicated the Au atoms must be located above the topmost Si layer. A related observation has been reported by Katayama *et al.*, who showed that the intensity of 180° backscattered He ions and neutrals at a 60° polar angle is independent of the azimuthal angle for scattering from Au, but is highly anisotropic for scattering from Si.[30]

In order to analyze the lateral arrangement of the Au atoms at the $\sqrt{3}\times\sqrt{3}$ and $6\times6$ (Si(111)/Au surfaces, we collected ICISS angular distributions for $Li^+$ elastically scattered from Au atoms along the $[1\,1\,\bar{2}]$, $[\bar{1}\,\bar{1}\,\bar{2}]$, $[1\,\bar{1}\,0]$, and $[\bar{1}\,1\,0]$ azimuths. The results are plotted in Figs. 4 and 5 for the two structures with the backscattered-ion yield as a function of the polar angle between the ion beam and the sample surface. Since the $[\bar{1}\,1\,0]$ and $[1\,\bar{1}\,0]$ azimuths are crystallographically equivalent and produced essentially identical angular scans, only the results measured in the $[\bar{1}\,1\,0]$ azimuth are shown in Figs. 4(b) and 5(b). The $[1\,1\,\bar{2}]$ and $[\bar{1}\,\bar{1}\,2]$ azimuths are related by a 180° rotation about the surface normal. They are not equivalent to each other when considering the bulk symmetry of Si, but the intensity variations observed in the ICISS scans from Au atoms were also essentially identical for these two azimuths. Therefore, only the ICISS polar scans collected along the $[1\,1\,\bar{2}]$ azimuth are shown in Figs. 4(a) and 5(a). The fact that the $[1\,1\,\bar{2}]$ and $[\bar{1}\,\bar{1}\,2]$ azimuths produced identical ICISS scans means that the Au atoms sit either in high symmetry sites, or that there are two different lower symmetry sites related by a mirror reflection in a $(1\,1\,\bar{2})$ plane, which was proposed by Porter, Chang, and Tsong,[17] for $\sqrt{3}\times\sqrt{3}$ Si (111)/Ag. As shown in the next section, the latter possibility cannot explain the observed ICISS data for Au on Si(111).

The surface flux peaks in these polar scans resulted primarily from Au-Au and/or Si-Au atom pairs on the Si(111) surface, since Au atoms were exposed to ion projectiles at low polar angles by passing through the shadow cones[22] cast by neighboring Au or Si atoms. In Fig. 4(a), there is only a single flux enhancement (i.e., the sharp feature at around 10°), and thus only a single shadowing interaction along $[1\,1\,\bar{2}]$. This revealed that only

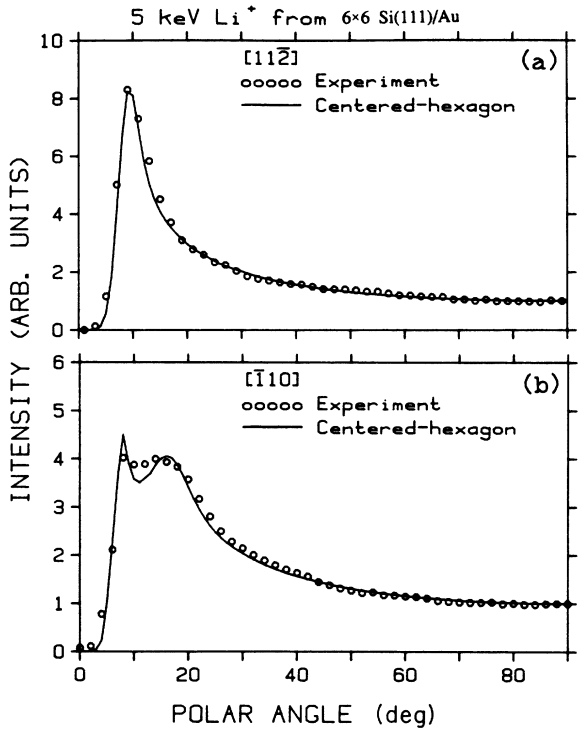


FIG. 5. Experimental ICISS polar scan (○) for 5-keV $Li^+$ scattering at 157° from the Au atoms on the 6×6 Si(111)/Au surface along the (a) [1 1 $\bar{2}$] and (b) [$\bar{1}$ 1 0] azimuths. The experimental angular distribution along the [1 1 $\bar{2}$] azimuth is essentially identical to that for the $\sqrt{3}\times\sqrt{3}$ surface, but the flux peak at low angle along the [$\bar{1}$ 1 0] azimuth is definitely broader than that for the $\sqrt{3}\times\sqrt{3}$ surface. The solid lines are the result of a calculation for the centered-hexagon model with the central atom 0.3 Å below the honeycomb plane.

one characteristic Au-Au or Si-Au interatomic distance is present along the [1 1 $\bar{2}$] azimuth for the $\sqrt{3}\times\sqrt{3}$ structure. If the Au atoms are located above the Si(111) surface, then Au-Au shadowing interactions must dominate the flux enhancement at low polar angle. Along the [$\bar{1}$ 1 0] azimuth [Fig. 4(b)], a broader flux enhancement that appeared to contain two unresolved peaks was observed. This was most likely the result of at least two shadowing effects caused by more than one type of Au-Au and/or Si-Au interatomic distance along the [$\bar{1}$ 1 0] azimuth. The focusing effect from the first type of atom pair gave rise to the flux enhancement with an onset at about 9°, and the focusing effect from a second type of atom pair (with a shorter interatomic spacing) gave rise to the second enhancement beginning at about 14° polar angle. Very similar ICISS data for the $\sqrt{3}\times\sqrt{3}$ structure led Oura *et al.*[14] to propose a trimer model for this surface but, as has been shown elsewhere[31] and later here, their model is actually not consistent with the experimental data. For the 6×6 structure, the ICISS polar scans (Fig. 5) are very similar to those for the $\sqrt{3}\times\sqrt{3}$ structure. This implies that the Au atoms in the $\sqrt{3}\times\sqrt{3}$ and 6×6 structures have nearly the same short-range order.

In order to determine the arrangement of Si atoms and the registry of the Au atoms with respect to the substrate in the $\sqrt{3}\times\sqrt{3}$ and 6×6 Au structures, we also examined the ICISS angular distributions for $Li^+$ ions elastically scattered from Si atoms along the [1 1 $\bar{2}$] and [$\bar{1}$ $\bar{1}$ 2] azimuths. The results are shown in Figs. 6 and 7 for the two structures as the backscattered-ion yield versus polar angle. As compared to the angular distribution for $Li^+$ scattered from Au atoms (Figs. 4 and 5), ICISS distributions from Si show very different overall flux features, and the [1 1 $\bar{2}$] and [$\bar{1}$ $\bar{1}$ 2] azimuths are different from each other.

The complicated angular distributions indicated that several Au-Si and/or Si-Si shadowing and blocking interactions overlapped. At higher polar angles, the three-dimensional structure of the Si substrate was clearly evident in the angular distributions because of the modulation of the backscattered yield from the second and deeper Si layers by shadowing and blocking interactions. Flux peaks at high polar angles were not observed in the $Li^+$ scattering from Au atoms, indicating that the Au was in the surface plane, and the extent of islanding for the coverages studied was negligible. ICISS polar scans for Si scattering from both the $\sqrt{3}\times\sqrt{3}$ and 6×6 structures again show nearly identical features along the [$\bar{1}$ $\bar{1}$ 2] azimuth (Figs. 6 and 7), which implied that the underlying Si atoms in the $\sqrt{3}\times\sqrt{3}$ and 6×6 reconstructions have essentially the same structure.

A simple analysis of the ion-scattering and LEED spot profile data enables the rejection of a large number of

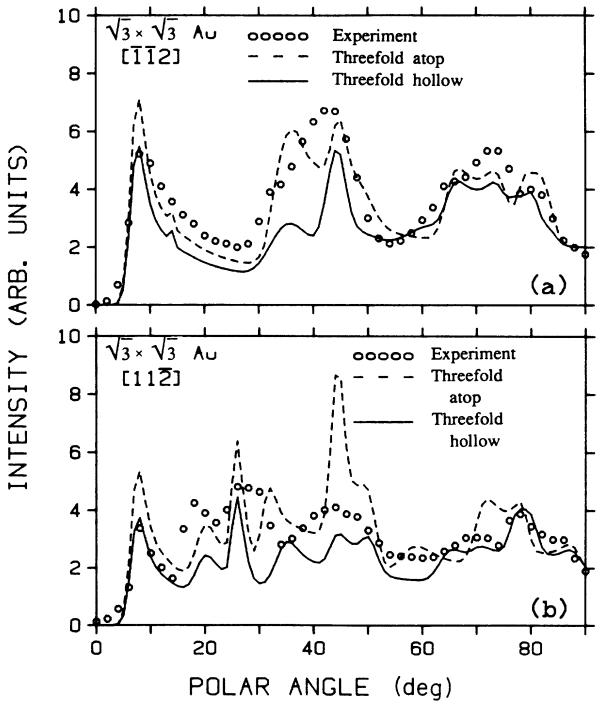


FIG. 6. Experimental ICISS polar scans (○) for 5-keV $Li^+$ scattering at 157° from the Si atoms on the $\sqrt{3}\times\sqrt{3}$ Si(111)/Au surface along the (a) [$\bar{1}$ $\bar{1}$ 2] and (b) [1 1 $\bar{2}$] azimuths. The lines are the result of calculations for the 70:30 model of $\sqrt{3}\times\sqrt{3}$Si(111)/Au (as described in the text) with Au atoms at threefold-hollow sites (——) and a honeycomb structure with Au atoms at threefold-atop sites (— — —).

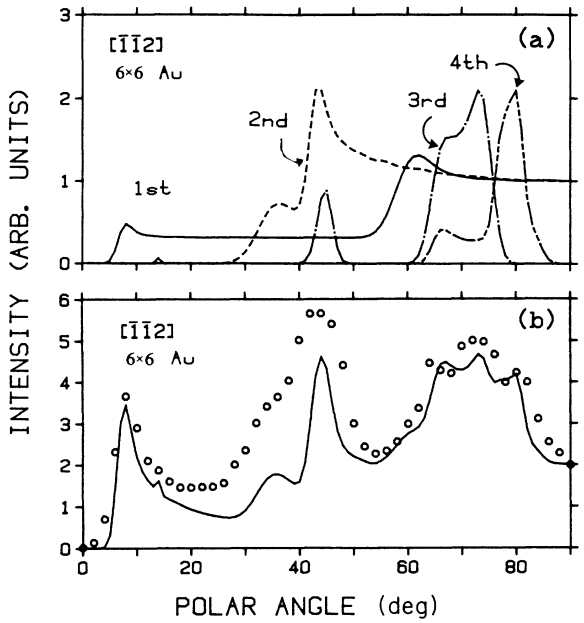


FIG. 7. (a) Calculated contributions for the ICISS scans from the first (——), second (— — —), third (–·–), and fourth (–·–·–) Si layers for the 20:80 model of 6×6 Si(111)/Au. (b) Experimental ICISS polar scan (○) for 5-keV $Li^+$ scattering at 157° from the Si atoms at the 6×6 Si(111)/Au surface along the [1̄ 1̄ 2] azimuth. The solid line is the result of summing over the top four layers (a).

models that have been proposed for the $\sqrt{3}\times\sqrt{3}$ and 6×6 surfaces. The two structures are very similar to each other, with the 6×6 having much better long-range order. The Au atoms most likely sit above the Si(111) surface in high symmetry sites. Thus the 6×6 structure is not related to Au-Si compound formation at the surface. Further consideration limits the possible adsorption sites to simple atop (which would be the termination of the Si dangling bond perpendicular to the surface), threefold hollow and threefold atop. Qualitative assignment of the flux peaks in the ICISS scans to certain atom pairs is possible by simple geometric analysis. However, because nonequivalent atom pairs may produce overlapping flux peaks (as shown in Figs. 4–7), calculations were necessary to choose among the adsorption sites and determine a quantitative structural model.

## IV. DISCUSSION AND QUANTITATIVE ANALYSIS

Computer simulations were performed for quantitative structural analysis of the ion-scattering data. A scattering probability model that has been successfully employed in analyzing the $NiSi_2$/Si(001) structure[26] was applied in this study. The essence of the method was to calculate the hitting probabilities in a two- or three-atom system, as discussed by Tromp and van der Veen.[27] The total scattered yield was regarded as the sum of encounters with an array of diatomic or triatomic molecules and was calculated for each atom group by determining the probability density that an incident ion could hit a target atom along a particular trajectory.[27] The results of the individual calculations were then combined together in the proper fashion[28,29] to simulate the desired crystal structure and scattering geometry, and the yield at each polar angle was divided by the sine of the polar angle to account for foreshortening. The algorithm for ICISS calculations is discussed further in Refs. 26 and 29.

The scattering angle as a function of impact parameter for $Li^+$ colliding with Au and Si was calculated using the Molière potential with the usual Firsov screening length multiplied by 0.735 for both Au and Si. The shadow cone size and therefore the angular position of the flux peaks depend on the value chosen for the screening length. In our calculations, the screening length was determined by choosing a constant to obtain the best agreement between the calculated and the experimental surface flux peaks, which is analogous to the internal calibration procedure of Aono for determining the shadow cone radius by measuring the critical angles of several different surface flux peaks.[22] The rms vibrational amplitudes used in these calculations were 0.126 Å for Au atoms and 0.0608 Å for Si atoms. The value for Si was the usual bulk rms vibrational amplitude. The value for Au was determined by finding the optimum agreement between the calculations and the experimental data and was found to be 1.4 times the vibrational amplitude for bulk elemental Au.

### A. Scattering from Au atoms

Model ICISS polar scans with 5-keV $Li^+$ scattering from Au have been calculated and reported[31] for six different previously proposed models for the $\sqrt{3}\times\sqrt{3}$ structure: (a) simple honeycomb[1] (illustrated in Fig. 8), (b) centered-hexagon[1] (Fig. 9), (c) simple Au atop with a 1-ML coverage, (d) trimer,[1,6,7,11–15] (e) surface-embedded

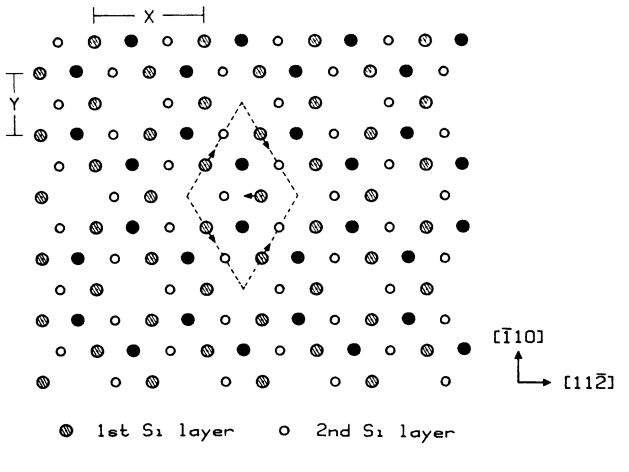


FIG. 8. A top view of the honeycomb structure for the $\sqrt{3}\times\sqrt{3}$ Si(111)/Au surface. The [1 1 2̄], [1̄ 1̄ 2], [1̄ 1 0], and [1 1̄ 0] are the major azimuths along which ICISS polar scans were collected. The top atomic plane is the Au overlayer (solid circles) followed by the first Si plane (hatched circles), and the second Si plane (open circles). The radii of the circles are drawn to represent the vibrational amplitudes of the atoms used in the calculations. $X$ represents a distance of 6.65 Å and $Y$ of 3.84 Å. A $\sqrt{3}\times\sqrt{3}$ unit cell is indicated by dashed lines.

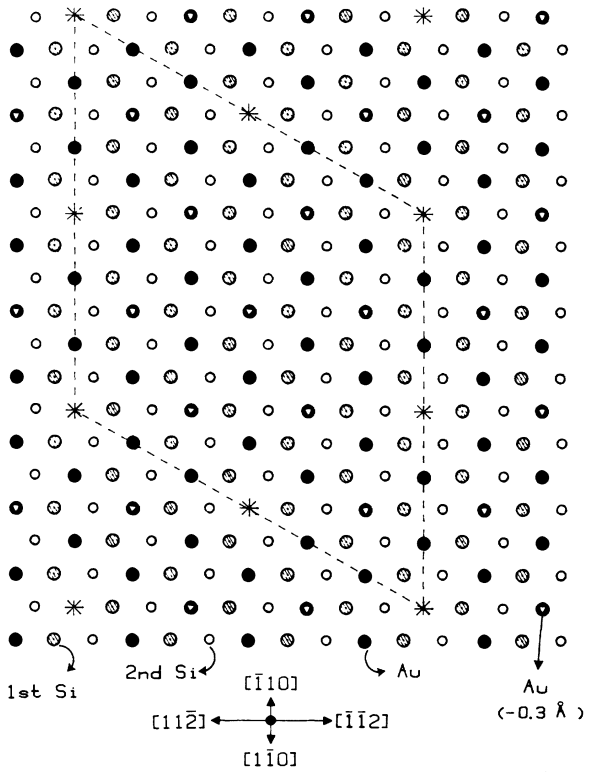


FIG. 9. A top view of the proposed model for the $6\times6$ Si(111)/Au surface. This is a honeycomb structure in which 75% of the Au hexagons have an additional Au atom in the center. The centered Au atoms (solid circles with inscribed triangles) sit slightly below ($-0.3$ Å) the other Au atoms in the hexagon array. The empty hexagon centers are indicated by a star, and the $6\times6$ unit cell is outlined by a dashed line.

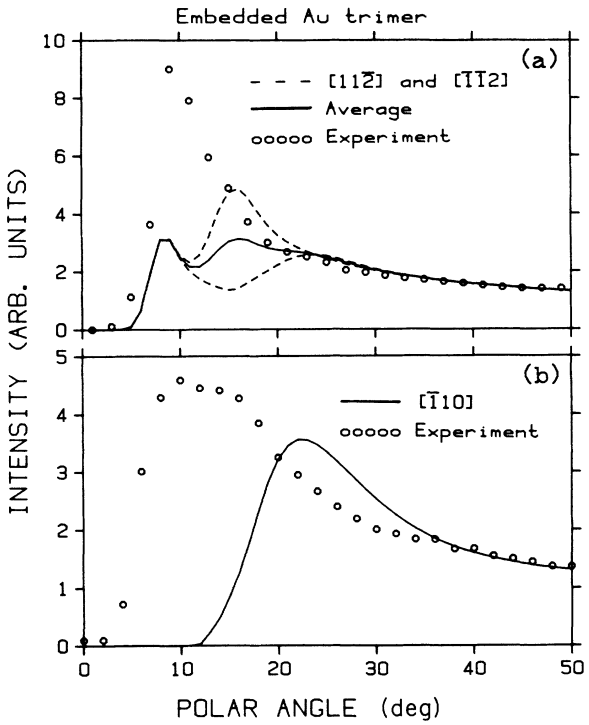


FIG. 10. Calculated ICISS polar scans for the surface-embedded Au trimer described in Ref. 17 along the (a) [1 1 $\bar{2}$] and [$\bar{1}$ $\bar{1}$ 2] (upper and lower dashed lines, respectively), and the average of the two azimuths (solid line), and (b) the [$\bar{1}$ 1 0] (solid line) azimuth. The experimental data for the relevant azimuths are also shown for comparison.

Au,[16,17] and (f) subsurface-immersed Au.[18] Models (c)–(f) were not consistent with the experimental ICISS data, but models (a) and (b) agreed quite well with the $\sqrt{3}\times\sqrt{3}$ $6\times6$ surfaces, respectively, and are compared to the experimental results in Figs. 4 and 5. The structure for the centered-hexagon model was the honeycomb array with the center of the Au hexagons occupied by other Au atoms slightly lower (0.3 Å) than those in the honeycomb plane.

Model ICISS calculations for a particular surface-embedded Au trimer [model (e)] proposed by Porter, Chang, and Tsong,[17] in which Au atoms of the trimer are displaced 0.7 Å from symmetric threefold sites and sit 0.7 Å below the Si(111) surface, are shown in Fig. 10 for the [1 1 $\bar{2}$], [$\bar{1}$ $\bar{1}$ 2], and [$\bar{1}$ 1 0] azimuths. This embedded-Au trimer yields different ICISS angular scans along the [1 1 $\bar{2}$] and [$\bar{1}$ $\bar{1}$ 2] azimuths, which disagrees with the experimentally observed results. However, if two different domains of trimers that are 180° out of phase with each other coexist, then the ICISS scans along the [1 1 $\bar{2}$] and [$\bar{1}$ $\bar{1}$ 2] would be equivalent. Such a two-domain average is compared to the experimental results in Fig. 10, but it disagrees severely with the experimental data, which has only a single, sharp flux enhancement for these azimuths. Thus there does not appear to be any way to reconcile the experimental results with subsurface Au atoms, whereas the honeycomb and centered-hexagon structures are extremely promising. For the honeycomb model in Fig. 8, the two different Au-Au distances (7.68 and 3.84 Å) along [$\bar{1}$ 1 0] naturally produce the broad flux enhancement in Fig. 4(b), as also observed for the experimental scan for the $\sqrt{3}\times\sqrt{3}$ structure. The agreement between the calculation and the experimental data was extremely good except for a slight discrepancy in the scattering intensity at the top of the surface flux peak.

The flux peak along the [$\bar{1}$ 1 0] azimuth for the $6\times6$ surface was broader than that for the $\sqrt{3}\times\sqrt{3}$, which indicated the presence of an additional type of atom pair that contributed to the scattered yield. To determine the height of the centered Au atoms in the centered-hexagon structure that best corresponded to the experimental results, both two-atom and three-atom calculations[29] were necessary to analyze the scattering events for an array of three Au atoms. The middle atom, corresponding to the one at the center of the hexagon, was slightly below the other two Au atoms along the [$\bar{1}$ 1 0] azimuth (shown in the inset of Fig. 11). Two Au-Au atom pairs in the surface plane separated by 7.68 and 3.84 Å and an atom pair out of the plane (distance depending on the height of the centered Au atom with respect to the honeycomb plane) were used to simulate the scattering from the centered-hexagon structure. The calculations presented in Figs. 11(a) and 11(b) are for the flux peaks that change with the position of the centered Au atom for distances 0.3–0.0 Å below the honeycomb plane. In Fig. 11(c), the sum of the scattering from all three atoms is shown.

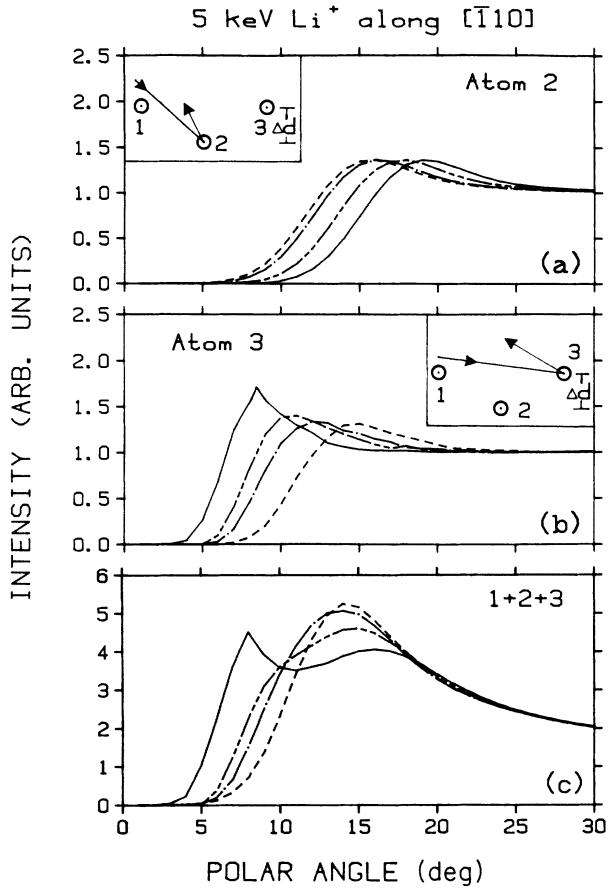


FIG. 11. Calculated flux peak for (a) atom 2 and (b) atom 3 in a three-atom array and (c) total ICISS distribution of the centered-hexagon model along the [$\bar{1}$ 1 0] azimuth with the centered Au atom, $\Delta d = 0.3$ (——), 0.2 (----), 0.1 (—·—·—), and 0.0 (— — —) Å below the Au atoms in the honeycomb plane.

Figure 11(a) shows the scattering from the centered atom (atom 2 in the inset), with the flux peak shifting towards a higher polar angle with increasing displacement of the centered Au atom. For scattering from the third atom in the array, the results of the three-atom calculations are shown in Fig. 11(b). The flux peak shifted towards a lower polar angle as a function of increased displacement of the centered Au atom. For a displacement larger than 0.3 Å, the result was identical to that for 0.3 Å since the middle Au atom in the three-atom array was then too distant to affect the scattering from the two atoms in the honeycomb plane. This trend in onset of the flux peak was just the opposite to that from atom 2 [Fig. 11(a)]. The total scattering distribution for the centered-hexagon model as a function of the centered Au atom displacement is plotted in Fig. 11(c). As can be seen in the figure, the width of the total flux peak was very sensitive to the displacement of the centered Au atom. The best agreement with the experimental data was obtained for a displacement of 0.3 Å. A change in the position of the centered Au atom by ±0.05 Å visibly degraded the agreement, which was fairly good except for a small discrepancy in the intensity at the top of the surface flux peak.

Under close examination, the experimental ICISS distributions along [$\bar{1}$ 1 0] from both the $\sqrt{3}\times\sqrt{3}$ and $6\times6$ structures appeared to fall between the calculated distributions for the simple honeycomb and the best centered-hexagon models. Therefore, weighted fractions of the honeycomb and centered-hexagon calculations were combined in order to obtain better agreement with the ICISS scans for both structures. The best agreements are shown as solid lines in Figs. 12(a) and 12(b) for the $\sqrt{3}\times\sqrt{3}$ and $6\times6$, respectively. For the $\sqrt{3}\times\sqrt{3}$ structure, the optimum weighting was 70% of the honeycomb and 30% of the centered-hexagon models, while for the $6\times6$ structure, 20% of the honeycomb and 80% of the centered-hexagon gave the best fit with the experiment. The combined models can be viewed as a simple honeycomb framework in which there are varying concentrations of extra Au atoms that sit in the center of the graphitelike hexagons of the honeycomb structure but at a slightly lower height. This model for the $\sqrt{3}\times\sqrt{3}$ surface was reasonable since an ideal honeycomb structure would be completed at $\frac{2}{3}$ ML of Au. The total Au coverage for the 70:30 mixture on a surface with a completed honeycomb lattice would be $0.67\pm0.3\times0.33=0.77$ ML, whereas the measured amount of Au deposited was 0.8 ML. The relative concentrations of these centered atoms for the two reconstructions was consistent with the fact that the $6\times6$

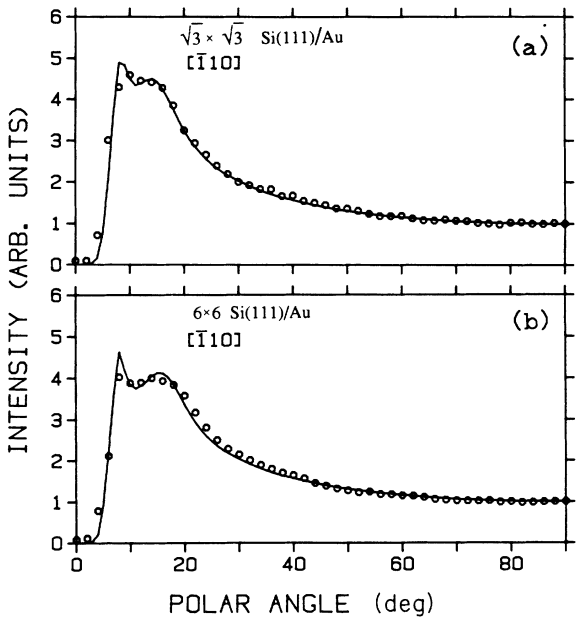


FIG. 12. Experimental ICISS polar scans (○) for 5-keV $Li^+$ scattered at 157° from the Au atoms on the (a) $\sqrt{3}\times\sqrt{3}$ and (b) $6\times6$ Si(111)/Au surfaces along the [$\bar{1}$ 1 0] azimuth. The solid line is the result of a calculation for a combination of (a) 70% of the honeycomb and 30% of the centered-hexagon models for the $\sqrt{3}\times\sqrt{3}$ structure and (b) 20% of the honeycomb and 80% of the centered-hexagon models for the $6\times6$ structure. The ordinate refers to the calculated intensity. The calculated distribution was normalized to the experimental intensity at the polar angle of 90°, at which there should be essentially no interatomic flux enhancement.

structure was formed at a higher total Au coverage, when more Au had been incorporated into the centers of the honeycomb hexagons. The total Au coverage for the $6\times6$ structure in the 20:80 mixture would be 0.93 ML, whereas the measured coverage was 1.1 ML. Since essentially all observers report that more than one monolayer of Au is required to form the $6\times6$ structure,[1-8] this reconstruction may require the presence of additional Au atoms (perhaps in islands) to stabilize the structure.

A very appealing model for the long-range order[32] of these surfaces is consistent with both the LEED patterns and the ICISS data. If the $6\times6$ structure is composed of a centered hexagon array with empty hexagons (i.e., honeycomb units) arranged on a $6\times6$ lattice as shown in Fig. 9, then 25% of the hexagons would be vacant, in close agreement with the the 20:80 combination of Fig. 12(b). The $\sqrt{3}\times\sqrt{3}$ structure is thus an incomplete $6\times6$ in which the centered and empty hexagons, which are both $\sqrt{3}\times\sqrt{3}$ unit cells, have no particular long-range order. This is consistent with the sharper LEED spots observed for the $6\times6$ structure. The idea of a mixed structure for the $\sqrt{3}\times\sqrt{3}$ surface was predicted by Julg and Allouche for Ag on Si(111)[12] and discussed by Le Lay.[1] The observations that the $\sqrt{3}\times\sqrt{3}$ and $6\times6$ structures must have very similar local order and the $\sqrt{3}\times\sqrt{3}$ changes nearly continuously into the $6\times6$ structure were also reported in the LEED studies of Higashiyama, Kono, and Sagawa.[19]

### B. Scattering from Si atoms

The lateral arrangement of the Au atoms was discussed in the previous section. A quantitative determination of the Au adsorption sites, Au atom heights above the Si plane, and the structure of the underlying Si atoms can be obtained by comparing the ICISS polar scans for 5-keV $Li^+$ scattered from Si atoms to computer simulations.

Calculations were mainly carried out for different Si structures with the Au atoms in honeycomb and centered-hexagon overlayers. Different Au adsorption sites consistent with the honeycomb arrangement, i.e., atop, threefold atop, and threefold hollow, were tested with varying Au atom heights with respect to the surface for bulk-terminated Si(111). Our results indicated that the two threefold sites gave similar results, and both agreed much better with the experimental data than the atop sites, in agreement with the theoretical results of Julg and Allouche for Ag/Si(111).[12] The calculations for both threefold-hollow and threefold-atop sites with a bulk Si(111) termination are compared to the experimental data for the $\sqrt{3}\times\sqrt{3}$ surface in Fig. 6 along the $[1\,1\,\bar{2}]$ and $[\bar{1}\,\bar{1}\,2]$ azimuths. Both models produced similar ICISS distributions along the $[\bar{1}\,\bar{1}\,2]$ azimuth [Fig. 6(a)], but the threefold-atop calculations were more intense in comparison to the experiment at several polar angles along $[1\,1\,\bar{2}]$ [Fig. 6(b)]. This is considered to be very unlikely, since the presence of extra Si reconstruction, disorder, or multiple scattering at the real surface should always lead to a more intense experimental scattered-ion yield at off-normal incidence than a calculation for an "ideal" surface. Thus for the $[1\,1\,\bar{2}]$ azimuth on the $\sqrt{3}\times\sqrt{3}$ surface, the threefold-hollow site was in better agreement with the experimental data than the threefold-atop site, in agreement with the SEXAFS results for Si(111)/Ag.[11] Various stacking fault structures[33] with reconstruction down to the fourth Si layer were also considered with Au atoms in threefold sites, but they failed to agree even qualitatively with the experimental ICISS scans.

A side view of the centered-hexagon structure along the $[1\,1\,\bar{2}]$ and $[\bar{1}\,\bar{1}\,2]$ azimuths is shown in Fig. 13, which presents Au atoms in the threefold-hollow sites (above the fourth Si layer) with respect to the underlying Si(111) surface. Along the $[1\,1\,\bar{2}]$ and $[\bar{1}\,\bar{1}\,2]$ azimuths in the centered-hexagon structure, there are two kinds of $[\bar{1}\,1\,0]$ planes (*a* and *b*), with twice as many *a* planes as *b* planes. Plane *a* has the Au atoms located 2.0 Å above the Si surface [Fig. 13(a)], and in plane *b* the Au atoms are 0.3 Å lower than those in plane *a* [Fig. 13(b)]. The simple honeycomb can also be represented in Fig. 13 if all the overlying Au atoms are absent in plane *b* [Fig. 13(b)].

Based on the optimum combination of honeycomb and centered-hexagon units determined in the previous section, a mixture of 70% of the honeycomb and 30% of the centered hexagon hexagon was compared to the Si ICISS data in Fig. 6 for the $\sqrt{3}\times\sqrt{3}$ Au structure, and 20% of the honeycomb and 80% of the centered-hexagon was compared to the Si data in Fig. 7 for the $6\times6$ Au structure. In both structures along the $[\bar{1}\,\bar{1}\,2]$ azimuth, the surface flux peak at a polar angle of 10° was mainly due to first-Si-layer to first-Si-layer focusing. Another flux peak at 62° was due to Au to first-Si-layer shadowing [tra-

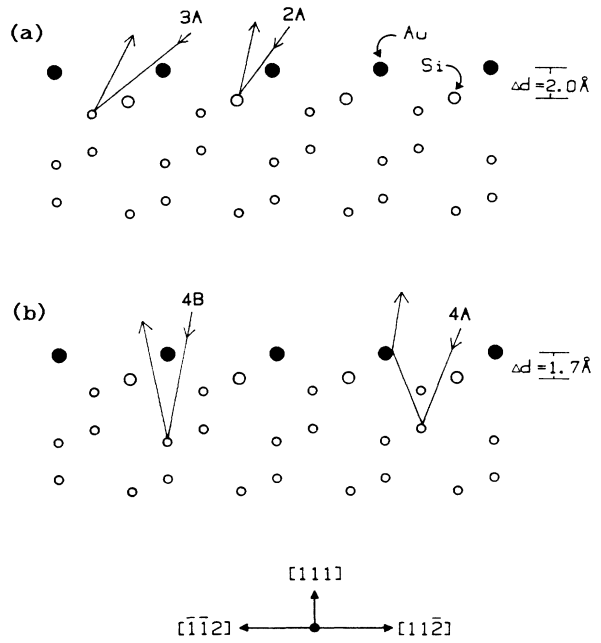


FIG. 13. The two different Si($\bar{1}\,1\,0$) planes of the bulklike Si(111) along the $[1\,1\,\bar{2}]$ and $[\bar{1}\,\bar{1}\,2]$ azimuths with the centered-hexagon arrangement of Au atoms (a) $\Delta d=2.0$ Å and (b) $\Delta d=1.7$ Å above the Si surface. The sizes of the Au atoms (solid circles) and Si atoms (open circles) are represented by the mean-square vibrational amplitudes used in calculations.

jectory $2A$ in Fig. 13(a)]. These two scattering events produced the distribution from the first Si layer in the Si($\bar{1}$ 1 0) plane, shown as a solid line in Fig. 7(a). For the second Si layer in the Si($\bar{1}$ 1 0) plane, the angular dependence of the scattered yield is shown as a dashed line in Fig. 7(a). A small flux peak at a polar angle of 35° involved the first-Si-layer to second-Si-layer shadowing, and Au to second-Si-layer shadowing also caused a flux peak at 44° [trajectory $3a$ in Fig. 13(a)]. The scattered yield from the third-Si-layer shows two major flux features: one at a polar angle of 45° and the other between 67° and 73°. These two features were mainly due to first-Si-layer to third-Si-layer shadowing and a combined shadowing and blocking effect involving the second and third Si layers [trajectory $4A$ in Fig. 13(b)]. The scattering events for the fourth Si layer are represented as two broad features at 67° and 80°. The feature at 67° was caused by the second-Si-layer to the fourth-Si-layer shadowing, and the feature at 80° was due to combined shadowing and blocking effects from Au to the fourth Si layer.

As shown in Figs. 6 and 7, the calculations reproduced all the scattering features and the peak positions. However, the experimental features were broader at the lower polar angles. This was most likely due to a slight reconstruction in the first one or two Si layers from their bulk positions. This buckling of Si atoms is expected to be small, however, since the agreement between the calculation based on the bulk Si(111) termination and the experimental data was reasonably good. In a study of the $5\times1$ Si (111) Au surface,[34] we have determined that Au atoms must sit at least 0.7 Å above the topmost Si layer if Au occupies threefold-hollow sites. In the present analysis, the optimum location of the honeycomb Au atoms was determined to be 2.0±0.2 Å above the Si plane in threefold-hollow sites. The large uncertainty in this determination is caused by the lack of detailed agreement between the calculations and the experimental data. There are contributions to the Si ICISS yield that were not included in the model calculations, such as multiple (i.e., more than three) atom scattering and possible slight displacements of Si atoms from their bulk lattice sites.

## V. SUMMARY AND CONCLUSIONS

Au films (about 0.8 and 1.1 ML) were evaporated onto several Si(111) substrates. The resulting reconstructions, the $\sqrt{3}\times\sqrt{3}$ and $6\times6$ structures, were studied by LEED and ICISS. The sharp LEED spots revealed that the ordered domains on these surfaces are fairly large. The length scale characteristic of the $\sqrt{3}\times\sqrt{3}$ structure was 340 and 610 Å for the $6\times6$ structure, which was thus much better ordered.

ICISS polar scans were analyzed by comparing them to two- and three-atom (with interplanar scattering if necessary) hitting-probability calculations. In the calculations, a Molière potential with the screening length reduced by 0.735 and rms vibrational amplitudes of 0.126 and 0.0608 Å for Au and Si, respectively, were used. The calculations provided an excellent understanding of the trajectories primarily responsible for the observed scattering features. In simulating the $Li^+$ scattering from Au atoms, the calculations reproduced the peak locations, relative shapes, and intensities in the ICISS polar scans nearly exactly (Figs. 4 and 5). This implied that the short-range order of the Au atoms was very regular. The identical angular distributions along the [1 1 $\bar{2}$] and [$\bar{1}$ $\bar{1}$ 2] azimuths for each reconstruction also indicated that Au atoms were located at high symmetry sites above the Si(111) surface. A mixture of two types of embedded trimers proposed by Porter, Chang, and Tsong[17] failed to explain the experimentally observed ICISS data for Si(111) Au.

A mixture of simple honeycomb and centered-hexagon units, with the centered atom 0.3±0.05 Å below the honeycomb plane, can explain both the $\sqrt{3}\times\sqrt{3}$ and $6\times6$ structures. The mixture of these two units is necessary to explain how extra Au atoms incorporate into the simple honeycomb structure, which is ideally completed at $\frac{2}{3}$ ML of Au, when both the $\sqrt{3}\times\sqrt{3}$ and $6\times6$ structures are observed at larger Au coverages. The $6\times6$ array of 25% empty hexagons in an otherwise centered-hexagon lattice in Fig. 9 is consistent with the LEED pattern and the ICISS results. The $\sqrt{3}\times\sqrt{3}$ structure is thus a precursor to the $6\times6$ in which the centered and empty hexagons have not formed a long-range superstructure. Since the Au overlayers in this study were extremely thin, the film could have been discontinuous. However, any gaps in the film would not affect the conclusions based on the Au atomic arrangement, since only backscattering from Au atoms was considered in that part of the data analysis. However, areas of exposed Si(111) could have affected the ICISS scans from Si and may in part be responsible for the discrepancies in the intensities and angular width between the model calculations and experimental data in Figs. 6 and 7.

The ICISS model calculations for $Li^+$ scattering from Si atoms were used to determine the adsorption site and positions of the Au atoms. The optimum Au atom height above the Si(111) surface was determined to be 2.0±0.2 Å in threefold-hollow sites for atoms in the honeycomb framework. The scattering results also indicated that Si atoms at the $\sqrt{3}\times\sqrt{3}$ and $6\times6$ Si(111)/Au surfaces were not displaced markedly from their ideal positions. According to Pauling's rule,[35] the Au-Si covalent bond length can be determined by the formula $R=2.5-0.6\log(n)$, where $n$ is the bond order. If $n=\frac{1}{3}$, i.e., Au is essentially single valent ($5d^{10}6s^1$) and interacts equally with the three nearest-Si dangling bonds, then the predicted bond length is 2.8 Å with an uncertainty of ±0.1 Å.[35] The bond length determined in this study is 3.0±0.3 Å, and thus agrees with the Pauling value, which may actually be more accurate. A slight distortion of the top-layer Si atoms from bulklike positions, as shown by the arrows in the $\sqrt{3}\times\sqrt{3}$ unit cell in Fig. 8, can account quite well for the difference in height of the honeycomb and the centered atoms above the Si plane. If the Au-Si bond length is assumed to be 2.8 Å for all the Au atoms on the surface, a displacement of the top-layer Si atoms in the directions shown in Fig. 8 (i.e., along [$\bar{1}$ $\bar{1}$ 2]-like directions) will open up the Si atoms forming the threefold-hollow site inside the Au hexagons. An Au atom bonding on this site will naturally reside 0.3 Å

lower than the Au atoms forming the honeycomb.

One of the most important results of this study was to show that the presence of submonolayer Au films can be easily detected at the Si(111) surface by LEIS, because of the large-Au-scattering cross sections. We were able to determine the structures for submonolayer Au reconstructions formed at the Si(111) surface, namely the $\sqrt{3}\times\sqrt{3}$ and $6\times6$. Any penetration of the Si surface by Au atoms would have been evident in this study. The quality of the agreement between the model ICISS calculations and the experimental data indicated that our model of the mixture of honeycomb and centered-hexagon units with the Au atoms at threefold-hollow sites above a bulk-terminated Si(111) surface is quite sound. In addition, this model is consistent with the observations of Higashiyama for Au on Si(111),[19] who reported that the $\sqrt{3}\times\sqrt{3}$ phase changes continuously to the $6\times6$ phase, and the theoretical calculations by Julg and Allouche for Ag on Si(111).[12] Detailed LEED *I-V* analyses and/or STM studies are now required to confirm or refute the details of this unified model for the $\sqrt{3}\times\sqrt{3}$ and $6\times6$ reconstructions of Si(111)/Au.

## ACKNOWLEDGMENTS

This project was supported by the National Science Foundation under Grant No. DMR-85-21663. R.S.W. acknowledges additional support from the Alfred P. Sloan Foundation and the Camille and Henry Dreyfus Foundation.

[1]G. Le Lay, Surf. Sci. **132**, 169 (1983).
[2]A. Hiraki, Surf. Sci. Rep. **3**, 357 (1983).
[3]A. K. Green and E. Bauer, J. Appl. Phys. **47**, 1284 (1976).
[4]M. Morooka, H. Tomokage, H. Kitigawa, and M. Yoshida, Jpn. J. Appl. Phys. **24**, 133 (1985).
[5]S. Ino, Jpn. J. Appl. Phys. **16**, 891 (1977).
[6]M. Ichikawa, T. Doi, and K. Hayakawa, Surf. Sci. **159**, 133 (1985).
[7]G. Le Lay and J. P. Faurie, Surf. Sci. **69**, 295 (1977).
[8]Y. Yabuuchi, F. Schiji, K. Oura, and T. Hanawa, Surf. Sci. **131**, L412 (1983).
[9]M. Aono, R. Souda, C. Oshima, and Y. Ishizawa, Surf. Sci. **68**, 713 (1986).
[10]R. J. Wilson and S. Chiang, Phys. Rev. Lett. **58**, 369 (1987).
[11]J. Stohr, R. Jaeger, G. Rossi, T. Kendelewicz, and I. Landau, Surf. Sci. **134**, 813 (1983); J. Stohr and R. Jaeger, J. Vac. Sci. Technol. **21**, 619 (1982).
[12]A. Julg and A. Allouche, J. Quantum Chem. **22**, 739 (1982).
[13]N. Osakabe, Y. Tanishiro, K. Yagi, and G. Honjo, Surf. Sci. **97**, 393 (1980).
[14]K. Oura, M. Katayama, F. Shoji, and T. Hanawa, Phys. Rev. Lett. **55**, 1468 (1985).
[15]G. Le Lay, J. Crystal Growth **54**, 551 (1981).
[16]E. J. van Loenen, J. E. Demuth, R. M. Tromp, and R. J. Hamers, Phys. Rev. Lett. **58**, 373 (1987).
[17]T. L. Porter, C. S. Chang, and I. S. T. Tsong, Phys. Rev. Lett. **60**, 1739 (1988).
[18]M. Saitoh, D. Shoji, K. Oura, and T. Hanawa, Surf. Sci. **95**, 411 (1980).
[19]K. Higashiyama, S. Kono, and T. Sagawa, Jpn. J. Appl. Phys. **25**, L117 (1986).
[20]F. Salvan, H. Fuchs, A. Baratoff, and G. Binnig, Surf. Sci. **162**, 634 (1985).
[21]F. Wehding, H. Beckermann, and R. Niedermayer, Surf. Sci. **71**, 364 (1978).
[22]M. Aono, C. Oshima, S. Zaima, S. Otani, and Y. Ishizawa, Jpn. J. Appl. Phys. **20**, L829 (1981).
[23]M. Aono, Phys. Rev. B **2**, 374 (1984).
[24]R. Souda, M. Aono, C. Oshima, S. Otani, and Y. Ishizawa, Surf. Sci. **128**, L236 (1983).
[25]J. A. Yarmoff and R. S. Williams, Surf. Sci. **166**, 101 (1986).
[26]J. H. Huang, D. K. Shuh, R. S. Daley, and R. S. Williams, Surf. Sci. **186**, 115 (1987).
[27]R. M. Tromp and J. F. van der Veen, Surf. Sci. **133**, 159 (1983).
[28]K. Sato, S. Kono, T. Teruyama, K. Higashiyama, and T. Sagawa, Surf. Sci. **158**, 644 (1985).
[29]R. S. Daley, J. H. Huang, and R. S. Williams (unpublished).
[30]M. Katayama, E. Nomura, N. Kanekama, H. Soejima, and M. Aono (private communication).
[31]J. H. Huang and R. S. Williams, J. Vac. Sci. Technol. A **6**, 689 (1988).
[32]J. H. Huang and R. S. Williams (unpublished).
[33]P. A. Bennett, L. L. Feldman, Y. Kuk, and E. G. McRae, Phys. Rev. B **28**, 3656 (1982).
[34]J. H. Huang and R. S. Williams, Surf. Sci. (to be published).
[35]Linus Pauling, *The Chemical Bond* (Cornell University Press, Ithaca, New York, 1967).